

Probabilistic MRI Maps for the Presentation and Management of Intracranial Meningiomas

Benoit Hudelist, MD, MSc^{1,2} • Angela Elia, MD, MSc^{1,2} • Alessandro Moiraghi, MD, MSc^{1,2} • Clément Debacker, PhD² • Maïmiti Seneca, MSc¹ • Joseph Benzakoun, MD, PhD^{1,3} • Catherine Oppenheim, MD, PhD^{1,3} • Fabrice Chrétien, MD, PhD^{1,3} • Marc Zanella, MD, PhD^{1,2} • Alexandre Roux, MD, PhD^{*1,2} • Johan Pallud, MD, PhD^{*1,2}

* A.R. and J.P. are co-senior authors.

Author affiliations, funding, and conflicts of interest are listed at the end of this article.

See also commentary by Todea in this issue.

Radiology: Imaging Cancer 2026; 8(4):e250696 • <https://doi.org/10.1148/rycan.250696> • Content codes: 

Purpose: To develop a voxel-based, MRI-derived atlas of intracranial meningiomas and assess the voxelwise associations of location with clinical presentation, management strategy, and malignancy grade.

Materials and Methods: This single-center retrospective study (January 2000–December 2024) included adults with intracranial meningioma and pre-operative MRI scans. Lesions were manually segmented and normalized to the Montreal Neurological Institute 152 template space and analyzed with volume-adjusted permutation testing and false discovery rate correction.

Results: The final cohort comprised 1333 patients (mean age, 58 years \pm 13 [SD], 1064 female [79.8%] and 269 male [20.2%] patients) with 1676 intracranial meningiomas. Density analysis revealed a cluster in the anterior or middle skull base. Symptomatic presentation was localized to the bilateral motor and premotor cortex, deep frontobasal regions, and anteromedial skull base (26 141 voxels; maximum z score [max z] = 7.70; $q < .05$). Symptom-specific clusters included focal deficits in the left precentral and anteromedial junction of the skull base (3163 voxels; max z = 9.26; $q < .05$), epilepsy in the bilateral premotor region including supplementary motor area and middle frontal gyrus (929 voxels; max z = 5.89; $q < .05$), and radioclinical signs of elevated intracranial pressure in the deep right frontal and left cerebellar regions (19 066 voxels; max z = 7.62; $q < .05$). The resection probability was clustered in the anterior skull base, middle skull base, bilateral supplementary motor area, left precentral gyrus, and deep frontobasal regions (56 649 voxels; max z = 9.50; $q < .05$). Among resected tumors with available histology, tumors with a higher World Health Organization grade (grade 2–3) were localized to a right frontal cluster along the superior and middle frontal gyri (97 voxels; max z = 5.76; $q < .05$).

Conclusion: The voxelwise maps of 1676 meningiomas revealed that tumor location was associated with symptoms, resection probability, and malignancy grade.

Supplemental material is available for this article.

©RSNA, 2026

Meningiomas are the most common primary intracranial tumors of the central nervous system, representing approximately 40% of all primary brain tumors in adults, as reported by the Central Brain Tumor Registry of the United States (1–3). Tumor location is a critical determinant of patient management, because it influences clinical presentation, histomolecular characteristics, therapeutic strategies, malignancy grade, and outcomes (4–6). Current conventional anatomic labeling approaches (eg, skull base, convexity, or falcine/parasagittal classification) remain clinically useful for communication, broad risk stratification, and treatment planning because they are easily applicable across patients in both routine clinical practice and research settings, and they are readily understandable to clinicians and researchers (7,8). Conventional anatomic labels offer only a coarse taxonomy, however, and large, multicompartiment tumors may be misclassified owing to the necessary single-site assignment, thus biasing interpretation and masking fine-scale spatial effects (5,6,9–11). Unbiased, MRI-based voxel-based lesion mapping (VBLM) techniques can overcome such limitations by normalizing lesions to a common stereotactic template space, such as Montreal Neurological Institute, Talairach, or other standardized reference templates (12), and quantifying spatial density without relying on predefined categories, thereby overcoming common classification biases (9–11,13,14).

MRI-derived probabilistic brain atlases have been developed for gliomas (13,14) and for meningiomas (9–11), enabling VBLM and statistical analyses beyond those possible with categorical schemes. Previous meningioma atlas studies refined the preferential spatial distribution of tumors and explored associations with biologic features. Hirayama et al (10) primarily provided a lesion frequency map and three-dimensional rendering of 260 lesions, whereas Sun et al (11) extended voxelwise analyses to biologic characteristics, recurrence, and extent of resection in a surgical cohort and Patel et al (9) focused on histopathologic and molecular grade. However, prior studies did not provide a unified large-scale voxelwise assessment of clinically relevant variables such as focal deficits, epilepsy, signs of elevated intracranial pressure, management strategy, and malignancy grade.

In this study, we aimed to analyze the associations of tumor location with clinical presentation, therapeutic management, and outcomes through VBLM in a large and homogeneous cohort of patients with intracranial meningiomas.

Materials and Methods

The authors had full access to all the data and take responsibility for its integrity and the accuracy of the analyses. No conflicts of interest are declared. Patients included in this

Abbreviations

max z = maximum z score, VBLM = voxel-based lesion mapping, WHO = World Health Organization

Summary

A large MRI voxel-based atlas mapped intracranial meningioma distributions, linking location to symptoms, management, and malignancy grade, and provided a standardized spatial reference to anticipate presentation and guide clinical decision-making.

Key Points

- In a large voxel-based MRI atlas of 1676 meningiomas, tumor density peaked at the anterior and middle skull base.
- Symptoms were localized to distinct regions, including focal deficits in the precentral gyrus and anteromedial skull base (3163 voxels; maximum z score [max z] = 9.26; $q < .05$), epilepsy in the pre-motor and middle frontal regions (929 voxels; max z = 5.89), and elevated intracranial pressure in the frontobasal region and posterior fossa (19 066 voxels; max z = 7.62).
- Resection probability clustered in the anterior and middle skull base, bilateral supplementary motor area, precentral gyrus, and frontobasal regions (56 649 voxels; max z = 9.50); World Health Organization grade 2–3 tumors were more localized to frontal regions (97 voxels; max z = 5.76).

Keywords

Intracranial Meningioma, MRI Mapping, Brain Atlas, Skull Base, Neurosurgery

cohort have not been analyzed in prior publications on the same topic. The study was approved by an institutional review board (IRB No. 1:2024/53; No. IRB00011687). Informed consent was waived for this retrospective observational study in accordance with French regulations.

Study Design and Sample

Consecutive patients managed for meningioma were identified from the adult neurosurgical center of Sainte-Anne Hospital, GHU Paris Psychiatry & Neurosciences, Paris, France, between January 2000 and December 2024. Inclusion criteria were age 18 years or older, intracranial tumor, diagnosis of meningioma on the basis of blinded neuropathologic review in accordance with the 2021 World Health Organization (WHO) classification (15) and the cIMPACT-NOW update 8 (4) for surgical patients or blinded neuroradiologic review for nonsurgical patients, and available preoperative MR images, including those acquired with an isotropic three-dimensional contrast-enhanced T1-weighted sequence with a section thickness less than or equal to 1.5 mm. Exclusion criteria were spinal location, unavailable MRI data, and missing clinical and/or follow-up data.

Data Collection

The following variables were recorded at the time of meningioma diagnosis: age, sex, clinical presentation (signs of increased intracranial pressure, focal neurologic deficits including cranial nerve palsy, epileptic seizure, exophthalmos, subcutaneous mass, or incidental discovery), tumor volume (in cubic centimeters, on contrast-enhanced T1-weighted images), tumor side, brain-related edema (hyperintense area on fluid-attenuated inversion recovery images), mass effect

(defined as compression, displacement, or deformation ≥ 0.5 mm of lateral ventricles), venous/sinus infiltration (defined as the intraluminal location of the meningioma on contrast-enhanced MR images, excluding the cavernous sinus region), therapeutic management (watch-and-wait approach, surgery, or radiation therapy) corresponding to the initial management strategy determined after baseline imaging, WHO grade of malignancy obtained from the neuropathology report (4,15), and extent of resection (Simpson grade) obtained from surgical reports and perioperative imaging (16). Disease duration and prior cranial radiation therapy before MRI were not consistently available and thus, they were not analyzed as covariates. The tumor location was classified as either the skull base (spheno-orbital region, clinoid process, orbital roof, olfactory groove, planum and jugum sphenoidale, tuberculum sellae, cavernous sinus, sphenoid wing, petrous ridge, clivus, or foramen magnum) or convexity (convexity sites defined by the adjacent cortical areas).

Radioclinical signs of elevated intracranial pressure were adjudicated at diagnosis by two neurosurgeons (A.R. and J.P., each with more than 10 years of experience in neurosurgery). No systematic lumbar puncture or invasive intracranial pressure monitoring was performed. This variable captured MRI findings compatible with elevated intracranial pressure (eg, obstructive hydrocephalus, sulcal/basal cistern effacement, and brain shift) while demonstrating clinical concordance (eg, nausea or vomiting, headache, and papilledema). Contrast agent type and injection-to-acquisition delays were not standardized throughout the study period and were not consistently available in the records. Therefore, enhancement timing and delayed enhancement/contrast clearance analyses were not performed.

Imaging Processing

The imaging process is illustrated in Figure 1. Because images were acquired in routine practice over a long study period, scanner-specific acquisition parameters beyond the required isotropic three-dimensional contrast-enhanced T1-weighted sequence were heterogeneous and not consistently retrievable.

Meningioma segmentation

A single evaluator (B.H.) who was blinded to the clinical, therapeutic, and follow-up data manually segmented the meningioma components on preoperative images using Brainlab Elements software (version 6.3.0.27, 2022; Brainlab AG) using the brush tool in the three orthogonal planes, followed by section-by-section review and correction to refine tumor boundaries. Enhancing components and necrotic and/or calcified areas, when present, were combined to define the solid tumor volume, which served as the region of interest. Calcifications were not quantified as a separate imaging cofactor; when suspected on MRI, they were included in the region of interest to represent the full extent of the lesion. However, CT was not systematically available to standardize calcification assessments.

MRI database organization

The segmented and native sequences for each meningioma were exported in Digital Imaging and Communications in Medicine format and subsequently converted to Neuroimag-

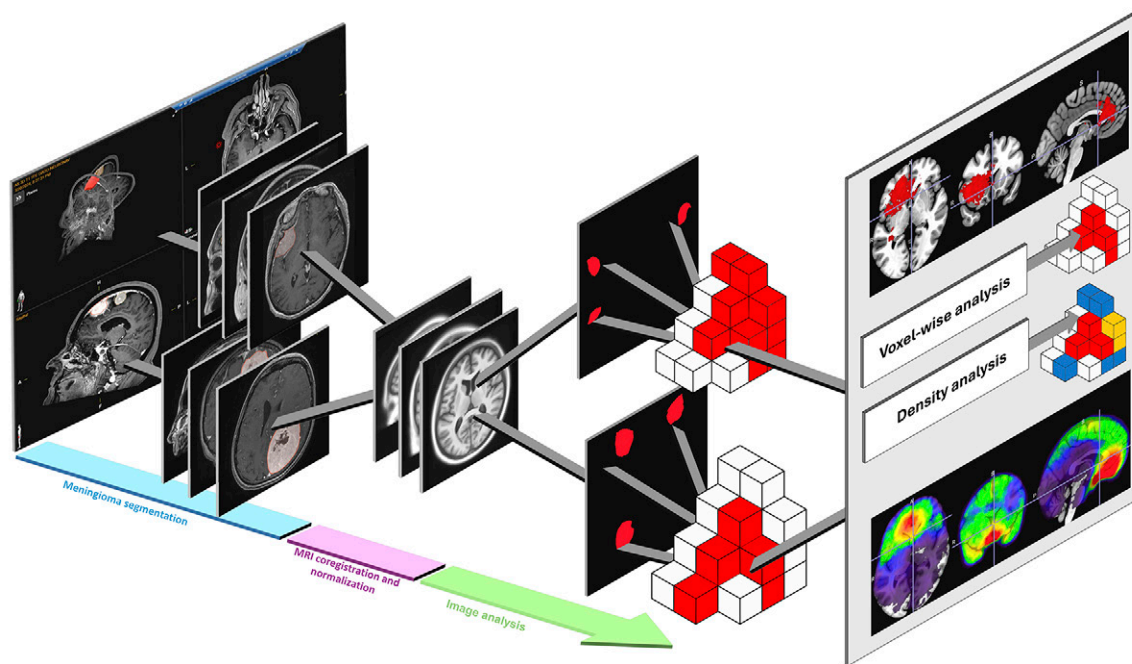


Figure 1: Image processing and voxelwise analysis pipeline. Contrast-enhanced T1-weighted MR images were segmented in Brainlab Elements (version 6.3.0.27; Brainlab AG) to generate the regions of interest (ROIs) of the meningiomas. Native and segmented datasets were exported, converted to Neuroimaging Informatics Technology Initiative format, organized according to the Brain Imaging Data Structure specification, and subsequently coregistered and normalized to the Montreal Neurological Institute 152 1-mm template using statistical parametric mapping software (SPM12; <https://www.fil.ion.ucl.ac.uk/spm/software/spm12/>) with MATLAB (version R2021b; MathWorks). The normalized ROIs were then analyzed with NiiStatGUI (MAC164; MATLAB version 9.11.0.2358333 [R2021b] Update 7; University of South Carolina) using two complementary approaches. First, density analysis was performed, corresponding to the cumulative overlap of all the voxels across meningiomas; the results are displayed as a frequency heatmap in which the color intensity indicates the number of meningiomas associated with each voxel. Second, a voxelwise analysis was conducted, consisting of statistical testing at each voxel to identify significant spatial associations between tumor location and clinical or surgical variables, with voxels highlighted to represent their statistical relevance.

ing Informatics Technology Initiative format. The MRI database was structured according to the international Brain Imaging Data Structure standard (<http://bids.neuroimaging.io>).

MRI coregistration and normalization

Image registration was performed using the open-source statistical parametric mapping 12 (SPM12; Functional Imaging Laboratory, Department of Imaging Neuroscience, University College London; <https://www.fil.ion.ucl.ac.uk/spm/software/spm12/>) software running on MATLAB (R2021b; MathWorks). MRI scans were spatially normalized in the Montreal Neurological Institute 152 template space and resampled to a 1.0-mm isotropic resolution using the SPM12 canonical International Consortium for Brain Mapping Montreal Neurological Institute 152 T1 template (avg152T1.nii) with the Clinical Toolbox tool (2017, Department of Psychology, University of South Carolina), which is designed to improve normalization of lesioned brains and the Diffeomorphic Anatomic Registration Through Exponentiated Lie Algebra (DARTEL, 2018, Wellcome Trust Centre for Human Neuroimaging), a high-dimensional nonlinear registration method (17). To ensure accurate alignment of lesioned brains, a cost-function masking approach was applied (18) that excludes the lesion from contributing to the normalization parameters, using a binary mask derived from the segmented tumor (17).

Quality assessment

Standardization was verified through an external quality control procedure (19,20). An external evaluator (M.S.), who

was blinded to the clinical, therapeutic, and follow-up data and the first segmentation, performed additional segmentations on the images of a random subset of 45 of 1333 patients (3.4%). This subset size was chosen pragmatically to permit full repeat manual segmentation while sampling cases across the study period and major tumor locations, in line with prior atlas/quality control approaches. Voxelwise agreement was assessed using the Pearson coefficient, and spatial overlap was evaluated using the Dice and Jaccard indexes. Missingness and potential selection bias related to exclusions and the number of meningiomas were assessed (Appendices S1 and S2).

Statistical Atlases

All segmented regions of interest were superimposed to generate three-dimensional location and frequency maps according to the parameters of interest. The frequency at each voxel in Montreal Neurological Institute 152 space was computed and color-coded for visualization using MRIcroGL software (2018, University of South Carolina). Three-dimensional renderings were produced using Surf Ice software (version 12.6; 2015, University of South Carolina). Group analyses focused on parameters related to clinical presentation (focal neurologic deficit, radiologic signs of elevated intracranial pressure, and epileptic seizures), treatment strategy, and malignancy grade in surgical patients (grade 1 vs grades 2–3). These parameters constituted the study outcomes in VBLM, with tumor volume included as an additional covariate in

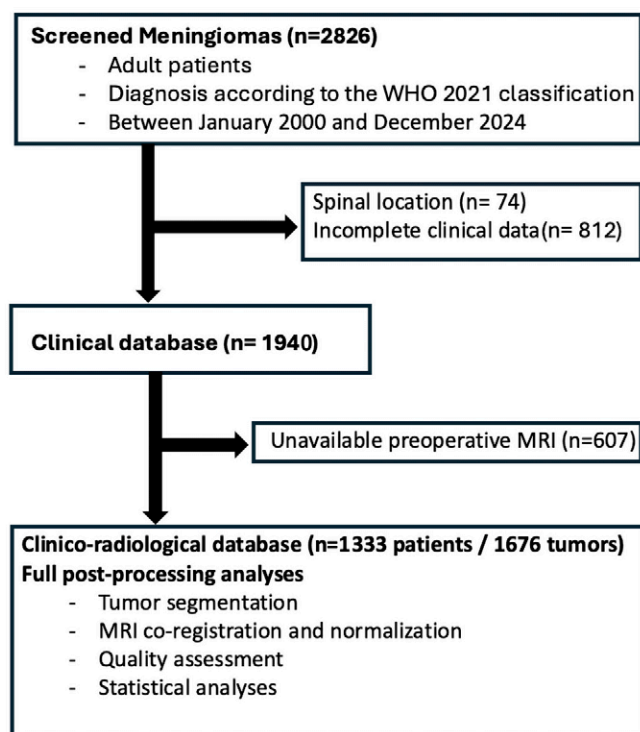


Figure 2: Flow diagram of selection study sample. WHO = World Health Organization.

all the models. The voxelwise framework targeted tumor location (lesion masks) rather than intratumoral imaging features; imaging features related to the tumor–brain interface, including the presence of a visible tumor–brain cleft (ie, preservation of a radiologic separation plane between the tumor and adjacent brain parenchyma), were not assessed as standardized variables.

Statistical Analysis

We assessed interrater reliability of the segmentation volumes using the Pearson correlation coefficient. The 95% CI for the Pearson correlation coefficient was calculated using the Fisher z transformation. Associations between regional meningioma involvement and parameters of interest were tested in a voxelwise manner within the VBLM framework. Each voxel was classified as inside or outside the region of interest, and its associations were analyzed against binary variables using the Liebermeister test or against continuous variables using generalized linear models. To avoid testing voxels with negligible lesion coverage, analyses were restricted to voxels covered by at least three tumors (minimal overlap $n = 3$); this is a voxel inclusion criterion and was not used as a cluster-extent threshold for inference. No cluster-extent threshold was applied to define statistical significance (21,22). Voxelwise analyses were performed using NiiStatGUI (MACI64; MATLAB version 9.11.0.2358333 [R2021b] Update 7; University of South Carolina). Voxelwise statistical significance was determined solely on the basis of multiple-comparison correction at the whole-brain level. The multiple testing problem was controlled for using nonparametric permutation testing ($n = 3000$ permutations) with voxelwise false discovery rate correction at $q = .05$. Associations were as-

essed in both directions; NiiStat reports direction-specific (one-tailed) permutation-derived thresholds for negative and positive z values, with voxelwise false discovery rate correction at $q = .05$. The random number generator seed was fixed and is reported, and the full analysis settings as well as scripts and parameter files are provided (Appendices S3 and S4). To mitigate lesion size confounding, all results of the voxelwise analyses were adjusted for the total tumor volume. Sensitivity analyses assessed robustness to exclusion-related missingness, within-patient clustering, and surgical selection. The primary voxelwise analyses were repeated in cohorts restricted to diagnoses from 2010 onward and from 2015 onward, and in a “one tumor per patient” cohort excluding patients with multiple meningiomas. Because WHO grade was available only for resected tumors, grade mapping was also repeated in a high-propensity surgical subset (predicted probability of surgery ≥ 0.70) derived from a multivariable logistic model including age, sex, tumor volume, skull base location, brain edema, and mass effect. Statistical analyses were performed using JMP software (version 18.0.2; SAS Institute).

Results

Study Sample Characteristics

A total of 2826 patients with meningiomas were managed at our institution during the study period. Among these patients, 74 patients were excluded because their tumors were located in the spine, 812 because of missing clinical or follow-up data, and 607 because of unavailable MRI data. The final cohort comprised 1333 patients with 1676 intracranial meningiomas (86.7% of patients presented with a single meningioma) (Fig 2).

The mean age of the patients was 58 years \pm 13 (SD), and 1064 of the 1333 patients were female (79.8%) (Table). The mean meningioma volume at discovery was 16.3 cm³ \pm 26.0, brain edema was present in 548 of 1676 tumors (32.6%), and mass effect was present in 473 of 1676 tumors (28.2%) (Table).

Segmentation Quality Was High

Voxelwise agreement between independent raters was excellent ($r = 0.987$; 95% CI: 0.98, 0.99). The Dice (0.90 \pm 0.05) and Jaccard (0.82 \pm 0.08) indexes further confirmed substantial spatial overlap. Lesion volumes were highly consistent, with a strong linear correlation in terms of the number of voxels (Fig 3). Agreement between raters was high across all segmentation metrics.

Voxel Density Peaked in the Anterior and Middle Skull Base

To characterize overall tumor distribution, we first generated descriptive density maps.

Meningiomas were most frequently located at the lateral convexity of the cerebral hemispheres (500 of 1676 tumors [29.8%]) and lateral skull base (including the sphenoidal region, clinoid process, orbital roof, sphenoid wing, and petrous ridge; 471 of 1676 tumors [28.1%]), followed by the midline convexity (including adjacent to the superior sagittal sinus and falcine sinus;

Study Sample Characteristics	
Characteristic	Value
Clinical parameters*	
Sex	
Female	1064 (79.8)
Male	269 (20.2)
Age (y), mean ± SD	58 ± 13
Symptom at diagnosis**	
Incidental discovery	663 (49.7)
Focal neurologic deficit	287 (21.5)
Epileptic seizure	202 (15.2)
Radioclinical signs of elevated intracranial pressure	234 (17.6)
Meningiomas per patient*	
1	1158 (86.7)
2	106 (8.1)
≥3	69 (5.1)
MRI characteristics at diagnosis‡	
Tumor volume (cm ³), mean ± SD	16.3 ± 26.0
Regional location [§]	
Lateral skull base	471 (28.1)
Midline convexity	362 (21.6)
Lateral convexity	500 (29.8)
Midline skull base	313 (18.7)
Other	30 (1.8)
Side	
Left	698 (41.6)
Right	687 (41.0)
Midline	291 (17.4)
Meningioma-related brain edema	
No	1128 (67.3)
Yes	548 (32.7)
Mass effect	
Yes	473 (28.2)
No	1203 (71.8)
Venous/sinus infiltration	
Yes	177 (10.6)
No	1499 (89.4)
Therapeutic management [‡]	
Watch and wait	935 (55.8)
Surgery	677 (40.4)
Radiation therapy	64 (3.8)
Follow-up (mo), median (95% CI) [‡]	51 (48, 60)
WHO grade of malignancy [#]	
1	403 (56.1)
2	247 (34.4)
3	68 (9.5)

Note.—Except where indicated, data are numbers, with percentages in parentheses. WHO = World Health Organization.

*Among all patients ($n = 1333$).

† The presence of multiple symptoms at diagnosis was possible.

‡ Among all meningiomas ($n = 1676$).

§ Lateral convexity (including cerebral hemispheres), lateral skull base (including sphenoid-orbital region, clinoid process, orbital roof, sphenoid wing, petrous ridge), midline convexity (including adjacent to superior sagittal sinus and falx), midline skull base (including olfactory groove, planum and jugum sphenoidale, tuberculum sellae, cavernous sinus, clivus, and foramen magnum), and other (including cerebellar convexity, optic nerve, intraventricular).

|| Defined by compression, displacement, or deformation of the ventricular system ≥ 0.5 mm.

For the 718 operated tumors (first- or second-line treatment).

362 of 1676 tumors [21.6%]) and midline skull base (including the olfactory groove, planum and jugum sphenoidale, tuberculum sellae, cavernous sinus, clivus, and foramen magnum; 313 of 1676 tumors [18.7%]).

Atlas-based density analysis (Fig 4) revealed a principal voxel cluster along the anterior (olfactory groove, planum and jugum sphenoidale, and orbital roof) and middle (sphenoid-orbital region, clinoid process, sphenoid wing, tuberculum sellae, and cavernous sinus) skull bases, comprising 11 732 voxels with a predominantly bilateral distribution.

Overall, voxel density was highest in the anterior and middle skull base.

Distinct Voxelwise Patterns Were Associated with Clinical Presentation

To assess whether tumor location was associated with clinical presentation, we performed voxelwise analyses for symptomatic presentation and major symptom groups.

Incidental discovery was the most common presentation (663 of 1333 patients [49.7%]), with several additional meningiomas incidentally discovered at MRI performed to diagnose a symptomatic meningioma. Among symptomatic patients, 287 of 1333 (21.5%) had focal neurologic deficits, 234 of 1333 (17.6%) had radioclinical signs of elevated intracranial pressure, and 202 of 1333 (15.2%) had epileptic seizures. Voxelwise analyses confirmed these associations, with voxel clusters associated with a symptomatic presentation, mainly in the convexity region, including the anteromedial skull base, in the motor and premotor regions on both sides, and in the deep frontobasal region (26 141 voxels; maximum z score [$\max z$] = 7.70; $q < .05$) (Fig 5).

Distinct symptom-specific voxel clusters were identified according to clinical presentation (Fig 6). For focal neurologic deficits (including cranial nerve palsy), two voxel clusters were identified, one surrounding the left precentral gyrus and another at the anteromedial junction of the skull base (sphenoid wing, planum and jugum sphenoidale, tuberculum sellae, clinoid process, and cavernous sinus) (3163 voxels; $\max z = 9.26$; $q < .05$). For epileptic seizures, a frontal premotor cluster (supplementary motor area and middle frontal gyrus) was identified bilaterally (predominantly left-sided) (929 voxels; $\max z = 5.89$; $q < .05$). For radioclinical signs of elevated intracranial pressure, two voxel clusters were identified: a deep right frontal cluster (caudate nucleus/adjacent frontal horn of the lateral ventricle) and a cluster along the left cerebellar hemisphere adjacent to the convexity dura (19 066 voxels; $\max z = 7.62$; $q < .05$).

Overall, symptom-related maps showed distinct spatial patterns according to presentation type.

Surgical Management Clustered in Skull Base and Frontal Motor Regions

To evaluate whether tumor location was associated with initial management strategy, we analyzed voxelwise patterns of surgical resection.

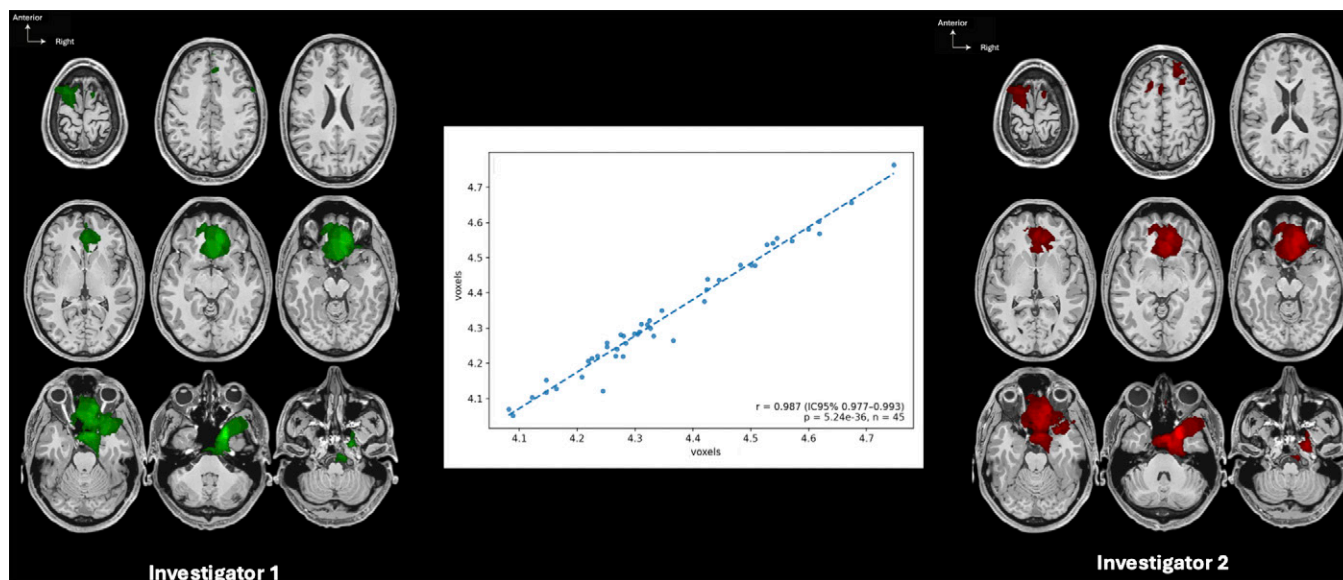


Figure 3: Segmentation quality assessment. To ensure robustness and assess interinvestigator variability, a comparison was performed. Forty-five patients were independently segmented by a second investigator (A.R.). Segmentation results are illustrated in the left panel for B.H. (investigator 1) and in the right panel for A.R. (investigator 2). Images are displayed in neurologic display convention. Agreement between the two raters was excellent ($r = 0.987$; 95% CI: 0.977, 0.993). Dice and Jaccard indexes demonstrated substantial spatial overlap, and lesion volumes were consistent across raters, with a strong linear correlation of voxel counts. These findings confirm the high reliability of the segmentation and normalization procedures, supporting data validity and minimizing interinvestigator bias.

Following discovery, 935 of 1676 meningiomas were managed conservatively with a watch-and-wait strategy (55.8%), while 677 of 1676 meningiomas underwent surgical resection (40.4%). Atlas-based analysis (Fig 7) revealed that surgical resection was clustered in the anterior skull base (olfactory groove, planum and jugum sphenoidale, and orbital roof), the middle skull base (spheno-orbital region, clinoid process, sphenoid wing, tuberculum sellae, and cavernous sinus), both frontal supplementary motor areas, the left precentral gyrus, and the deep frontobasal cluster (adjacent to the frontal horn of the lateral ventricle) (56 649 voxels; max $z = 9.50$; $q < .05$). The Simpson grade among surgical patients is described in Table S6.

Overall, resection-associated voxels clustered in the skull base and frontal motor regions.

Higher-Grade Tumors Localized to a Small Right Frontal Cluster

To examine whether location varied according to tumor grade, voxelwise grade analyses were restricted to resected tumors with available histology.

The grade of malignancy was available only after surgical resection; therefore, the voxelwise grade analyses were limited to resected tumors with available histologic analyses. Among the 718 meningiomas with available grades obtained after surgical resection (677 as first-line treatment, 41 after tumor growth following the initial watch-and-wait strategy), WHO grade 1 was most frequent (403 of 718 tumors [56.1%]), followed by grade 2 (247 of 718 tumors [34.4%]) and grade 3 (68 of 718 tumors [9.5%]). Atlas-based density maps of WHO grade 2 or 3 tumors versus grade 1 tumors (Fig 8) revealed a right frontal predominance along the superior and middle frontal gyri. Voxelwise analyses confirmed these patterns, with a voxel cluster along the right superior and middle frontal gyri that was significantly associated with

WHO grades 2 or 3 tumors versus WHO grade 1 tumors (97 voxels; max $z = 5.76$; $q < .05$).

However, because the malignancy grade can be determined only for resected tumors, this association may be influenced by surgical selection. In a sensitivity analysis restricted to a high-propensity resection subset (propensity score ≥ 0.70 ; $n = 403$), no voxels survived whole-brain corrected inference (Appendix S5). Overall, higher-grade tumors localized to a small right frontal cluster in the resected subset.

Discussion

Using a homogeneous MRI pipeline and voxelwise analyses, we generated a high-resolution three-dimensional atlas based on 1676 adult meningiomas. While meningiomas were most often in convexity regions according to crude counts, voxel-density mapping demonstrated their predominance in anterior and middle skull base regions, with a principal cluster comprising 11 732 voxels. For symptomatic meningiomas, voxels were distributed in the anteromedial skull base, the deep frontal region, and the bilateral motor and premotor cortices (26 141 voxels; max $z = 7.70$; $q < .05$). For focal neurologic deficits, voxels were distributed in the left precentral cortex and anteromedial junction of the skull base (3163 voxels; max $z = 9.26$; $q < .05$). For epilepsy, voxels were distributed bilaterally across the premotor and middle frontal cortices (929 voxels; max $z = 5.89$; $q < .05$). For radioclinical signs of elevated intracranial pressure, voxels were distributed in the deep right frontobasal region and left posterior fossa convexity (19 066 voxels; max $z = 7.62$; $q < .05$). Finally, for patients requiring surgical resection, voxels were distributed in the anterior skull base, the middle skull base, both frontal supplementary motor areas, the left motor cortex, and the deep frontobasal cluster (56 649 voxels; max $z = 9.50$; $q < .05$). Regarding the malignancy grade, voxels were distributed in the right frontal lobe (97 voxels; max $z = 5.76$; $q < .05$), along the superior and mid-

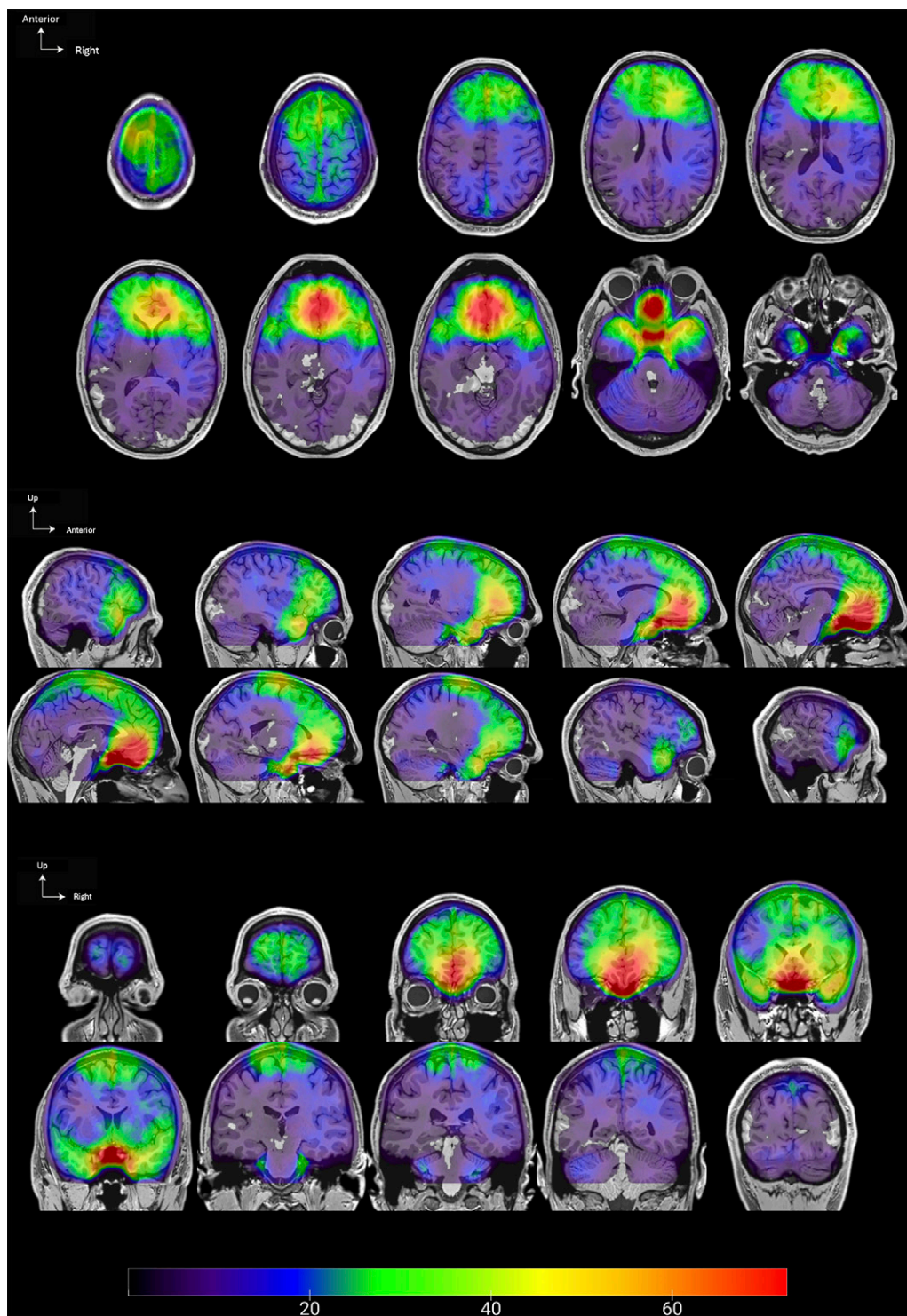


Figure 4: Location and frequency of meningiomas ($n = 1676$). Voxel density peaked in the anterior and middle skull base, with a predominantly bilateral distribution. The color frequency map indicates the number of meningiomas per voxel. Images are displayed in neurologic display convention.

dle frontal gyri for WHO grade 2 or 3 meningiomas. Taken together, these findings indicate that meningioma location is not merely descriptive, but is closely associated with clinical presentation and management, with a more exploratory signal for tumor grade.

Our atlas confirms a relative enrichment of meningioma voxels in the anterior and middle skull base and, more

broadly, in frontal and parasagittal predilection sites. This pattern is broadly consistent with previous atlas studies, which also identified preferential involvement of the skull base, parasagittal region, convexity, and frontal compartments (9–11,23). Hirayama et al (10) mapped lesion frequency and identified the middle third of the superior sagittal sinus, perisylvian convexity, and skull base as common locations.

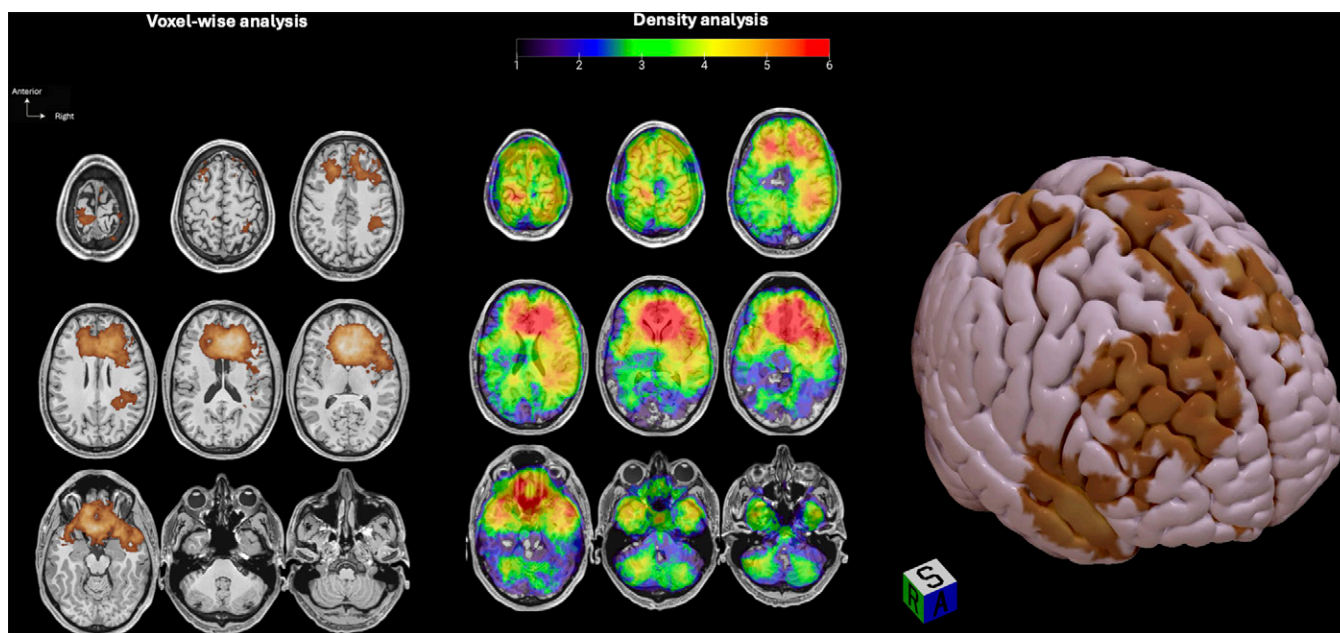


Figure 5: Density and voxelwise analysis of meningiomas with symptomatic presentations. The left panels show the density map of meningiomas in patients with symptomatic presentation. The center panels show the corresponding voxelwise map, with colored voxels (brown) indicating regions surviving whole-brain multiple-comparison correction ($q < .05$). The three-dimensional rendering illustrates the spatial distribution of suprathreshold voxels. Images are displayed in Montreal Neurological Institute 152 space using neurologic convention.

In a larger surgical cohort, Sun et al (11) similarly found frequent convexity and parasagittal locations and reported associations between location, resection status, recurrence, and histopathologic markers. Patel et al (9) also reported spatial differences according to WHO grade, with grade 1 tumors predominating at the anterior skull base and grade 3 tumors more often located in the convexity and sphenoid wing. Finally, Hosainey et al (23) reported population-level predilection sites in the frontal parasagittal region and frontal and middle skull base compartments. In our cohort, the grade-related signal was more limited and confined to a small right frontal convexity cluster, suggesting either cohort-specific differences or greater sensitivity of prior grade-related analyses to surgical selection.

More generally, previous atlases mainly described spatial distribution or biologic correlates, whereas the present study extends this literature by jointly assessing symptom, management, and grade associations within the same large voxelwise framework. The discrepancy between crude tumor counts and voxel-density concentration is also anatomically plausible, for the convexity covers a much larger dural surface, whereas skull base regions occupy smaller but proportionally more concentrated compartments. Together, these findings suggest that voxelwise atlases refine conventional site-based classifications by identifying clinically meaningful spatial subregions rather than broad anatomic labels alone.

To our knowledge, a voxelwise approach has not been applied to directly associate meningioma location with clinical presentation in any prior study. Our VBLM patterns are consistent with prior clinical series suggesting that meningioma-related symptoms are driven predominantly by mass effect and peritumoral edema. In Bommakanti et al (24), cognitive deficits were most frequent in frontal and temporal supratentorial meningiomas and were associated with larger tumor volume,

greater peritumoral edema, and raised intracranial pressure, in keeping with our voxelwise findings. Focal motor deficits were linked to voxels within the precentral and postcentral areas, which is consistent with the described susceptibility of the cortico-subcortical motor network to external compression and edema (25). A left predominance may reflect proximity to language-related networks, although no voxels in the perisylvian and fronto-opercular regions reached significance. Skull base presentations are readily explained by cranial nerve involvement, especially within the anterior and middle fossae. Deep voxel-cluster localizations in our map were associated with radioclinical signs of elevated intracranial pressure. By expanding into deep compartments, large extra-axial masses decrease intracranial compliance, compress neurovascular structures, crowd basal cisterns, and increase intracranial pressure. In the posterior fossa, even moderate lesions can compromise the fourth ventricular outlets or the cerebral aqueduct, precipitating acute obstructive hydrocephalus (24). Consistent with the literature, in the present study epilepsy was predominantly associated with non-skull base regions, cortex-adjacent meningiomas, and peritumoral edema (26). The localization of meningiomas to bilateral, although predominantly left, frontal voxels in our VBLM aligns with the voxelwise data, which indicated that the premotor cortex was a key area associated with epilepsy, and meta-analytic evidence, according to which non-skull base regions are strongly associated with epilepsy (26,27). Mechanistically, rather than parenchymal invasion, mass effects and brain edema are likely to drive cortical irritability within prefrontal networks (28–30). Overall, these findings support the clinical relevance of voxelwise symptom maps for identifying neuroanatomically vulnerable regions and for anticipating meningioma-related presentation.

This grade-related signal should be interpreted with caution, because no voxels survived whole-brain corrected inference in the

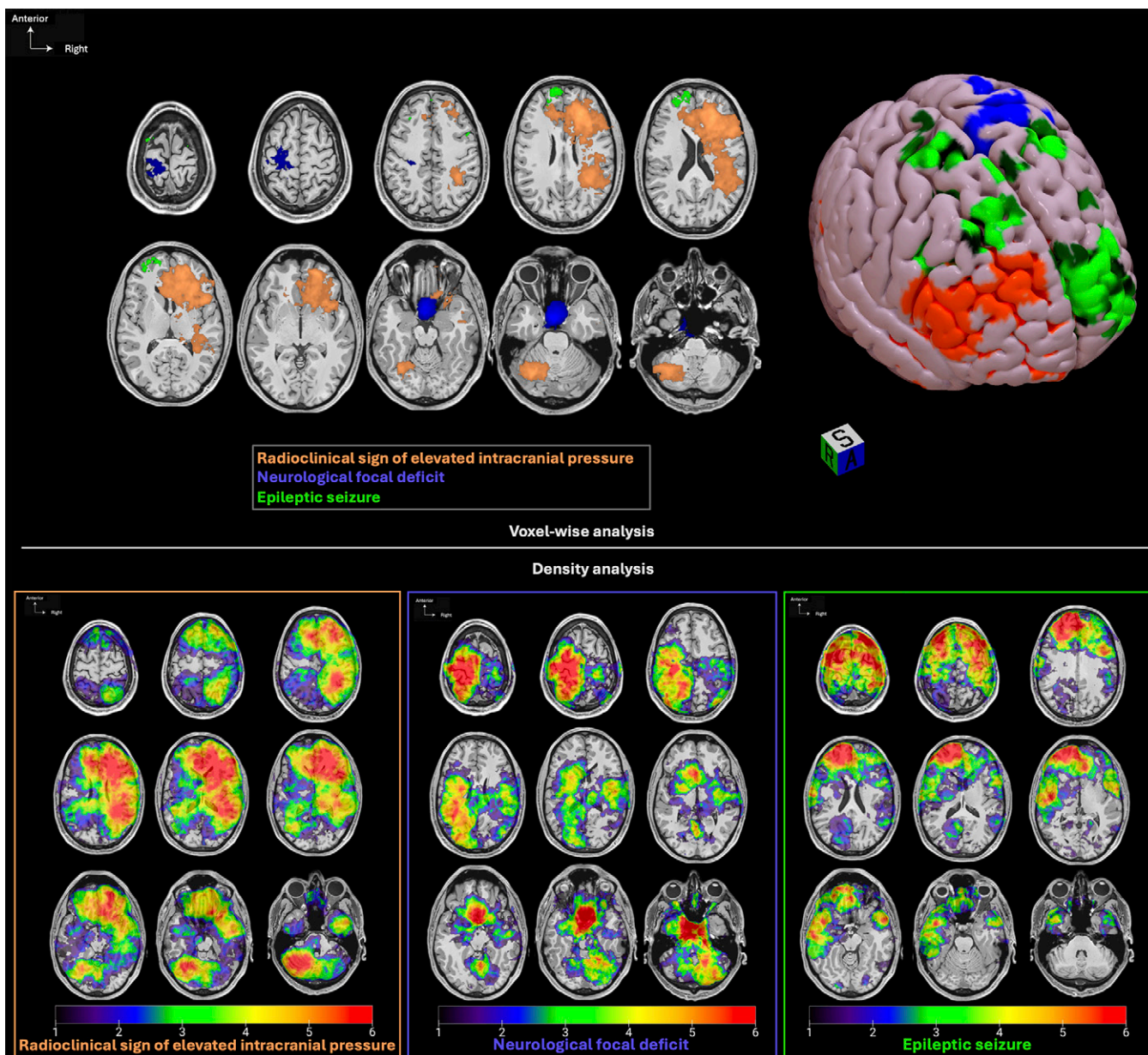


Figure 6: Probability map of meningioma location according to clinical presentation. Separate voxelwise maps are shown for focal neurologic deficit (blue), epileptic seizure (green), and radioclinical signs of elevated intracranial pressure (orange). Colored voxels indicate regions surviving whole-brain multiple-comparison correction ($q < .05$). The color frequency map indicates the number of meningiomas involving each voxel. Images are displayed in Montreal Neurological Institute 152 space using neurologic convention.

sensitivity analysis restricted to tumors with a high propensity for surgery (propensity score ≥ 0.70). The reason for this apparent right frontal predominance remains unknown. Prior studies suggest that brain tumors are generally not expected to show marked hemispheric asymmetry. Several explanations may be considered, including chance or sample-specific selection effects (31). However, evidence remains insufficient to support any firm explanation, and thus, this observation should be interpreted cautiously.

The study limitations include the retrospective single-center design, the exploratory nature of the analyses, the lack of an external validation set, and heterogeneity in MRI acquisition (sequences, scanners, and lower-quality earlier examinations). To mitigate acquisition-related variability, we applied minimal imaging inclusion standards. Selection bias is also possible because some patients were included based on imaging diagnosis without

histopathologic confirmation. Although we used cost-function masking during spatial normalization to reduce tumor-related distortion, the clinically relevant mass effect may still have limited registration accuracy. While all the results of the voxelwise analyses were adjusted for total tumor volume to mitigate lesion size confounding, descriptive voxel-frequency maps remain inherently weighted by lesion size; thus, larger anterior skull base tumors may appear overrepresented, despite the volume adjustment, owing to collinearity between size and location. Accordingly, frequency maps should be interpreted as voxel-level coverage rather than tumor-level prevalence. Because tumors were segmented only at diagnosis, we could not quantify longitudinal growth rates, particularly for asymptomatic tumors that were initially managed with observation. Thus, predictors of the transition from the watch-and-wait strategy to surgery could not be

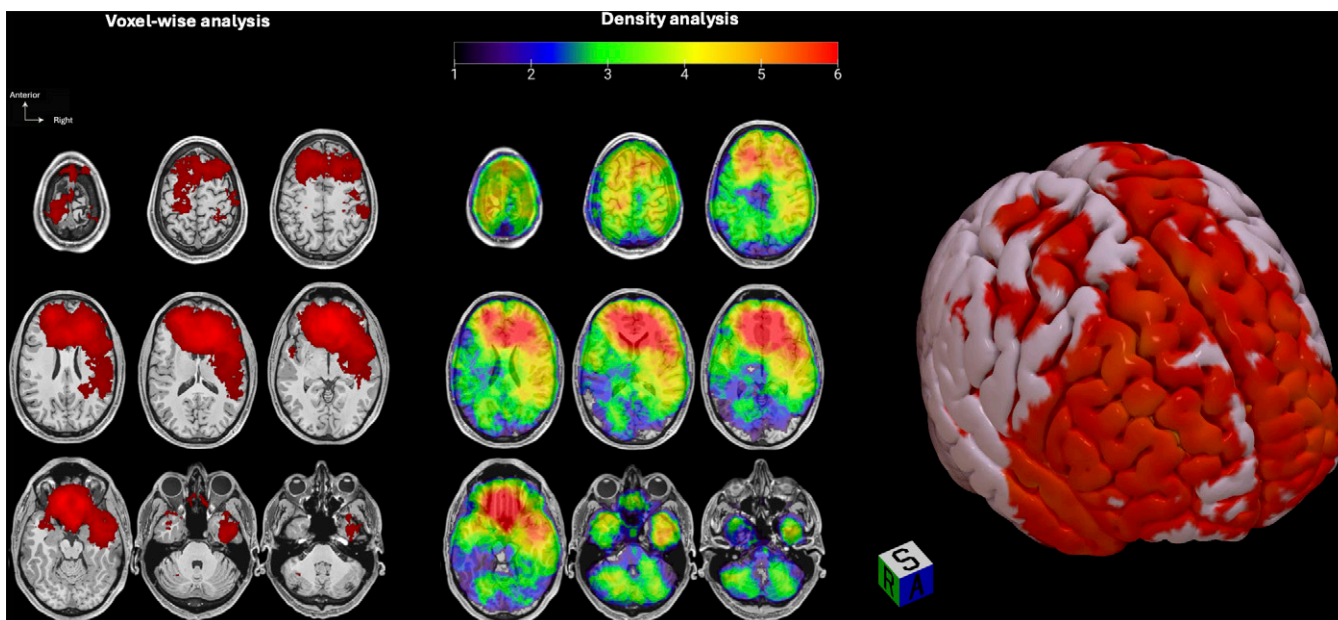


Figure 7: Density and voxelwise analysis of meningiomas for surgical management. The left panels show the density map of meningiomas managed surgically. The center panels show the corresponding voxelwise map, with colored voxels (red) indicating regions surviving whole-brain multiple-comparison correction ($q < .05$). The three-dimensional rendering illustrates the spatial distribution of suprathreshold voxels. Images are displayed in Montreal Neurological Institute 152 space using neurologic convention.

robustly investigated. Finally, the gadolinium-based agent type and injection-to-acquisition delay were not standardized and were inconsistently retrievable; thus, we did not assess enhancement timing or late-enhancement/contrast clearance patterns. A formal patient-level random-effects voxelwise model was not implemented; accordingly, within-patient dependence was addressed only partially through a “one tumor per patient” sensitivity analysis. In the tumor-level inference, uncertainty may be underestimated owing to within-patient dependencies. Because the WHO grade was available only for resected tumors, grade–location associations are subject to surgical selection and are reported as descriptive/exploratory results for this subset. Grade information is not available for tumors that were not managed surgically, and propensity-weighted approaches rely on strong, unverifiable assumptions; thus, we did not perform propensity-based reweighting.

To our knowledge, this study provides the largest voxel-based, MRI-derived atlas of the intracranial meningioma distribution to date, integrating detailed clinical and imaging data. Our results highlight distinct spatial patterns according to clinical presentation and management strategy. Symptom-specific voxel patterns suggest close anatomic relationships between tumor location and symptoms. These findings underscore the importance of considering anatomic distribution in the clinical assessment of meningiomas, both for anticipating symptoms and for informing management decisions. The proposed atlas offers a standardized spatial reference that may support future studies investigating location-related biologic, clinical, and molecular determinants of meningioma behavior.

Author affiliations:

¹ Service de Neurochirurgie, GHU-Paris Psychiatrie et Neurosciences, Site Sainte Anne, 1 rue Cabanis, 75014 Paris, France

² Institute of Psychiatry and Neuroscience of Paris (IPNP), Université Paris Cité, INSERM U1266, IMA-Brain, Paris, France

³ Service de Neuroradiologie, GHU-Paris Psychiatrie et Neurosciences, Site Sainte Anne, Paris, France

Received November 11, 2025; revision requested December 30; revision received March 19, 2026; accepted April 22.

Address correspondence to: J.P. (email: johanpallud@hotmail.com).

Supplemental material: Supplemental material is available at *Radiology: Imaging Cancer* online.

Funding: Authors declared no funding for this work.

Author contributions: Benoit Hudelist: Data curation, Formal analysis, Investigation, Methodology, Visualization, Writing - original draft, Writing - review & editing; Angela Elia: Writing - original draft, Writing - review & editing; Alessandro Moiraghi: Writing - original draft, Writing - review & editing; Clément Debacker: Formal analysis, Methodology; Maïmiti Seneca: Formal analysis; Joseph Benzakoun: Writing - original draft; Catherine Oppenheim: Writing - original draft; Fabrice Chrétien: Writing - review & editing; Marc Zanello: Writing - original draft, Writing - review & editing; Alexandre Roux: Writing - original draft, Writing - review & editing; and Johan Pallud: Conceptualization, Formal analysis, Investigation, Methodology, Project administration, Supervision, Validation, Visualization, Writing - original draft, Writing - review & editing.

Acknowledgments: The authors would like to thank the AMAVEA association for its support in the realization of this study.

Disclosures of conflicts of interest: Please see ICMJE form(s) for author conflicts of interest. These have been provided as supplemental materials.

References

1. Wang JZ, Landry AP, Raleigh DR, et al; International Consortium on Meningiomas (ICOM). Meningioma: International Consortium on Meningiomas consensus review on scientific advances and treatment paradigms for clinicians, researchers, and patients. *Neuro Oncol* 2024;26(10):1742–1780.
2. Ogasawara C, Philbrick BD, Adamson DC. Meningioma: A Review of Epidemiology, Pathology, Diagnosis, Treatment, and Future Directions. *Biomedicines* 2021;9(3):319.
3. Ostrom QT, Price M, Neff C, et al. CBTRUS Statistical Report: Primary Brain and Other Central Nervous System Tumors Diagnosed in the United States in 2016–2020. *Neuro Oncol* 2023;25(12 Suppl 2):IV1–IV99.
4. Sahm F, Aldape KD, Brastianos PK, et al. cIMPACT-NOW Update 8: Clarifications on molecular risk parameters and recommendations for WHO grading of meningiomas. *Neuro Oncol* 2025;27(2):319–330.
5. Splavski B, Hadzic E, Bagic I, Vrtrac V, Splavski B. Simple Tumor Localization Scale for Estimating Management Outcome of Intracranial Meningioma. *World Neurosurg* 2017;104:876–882.

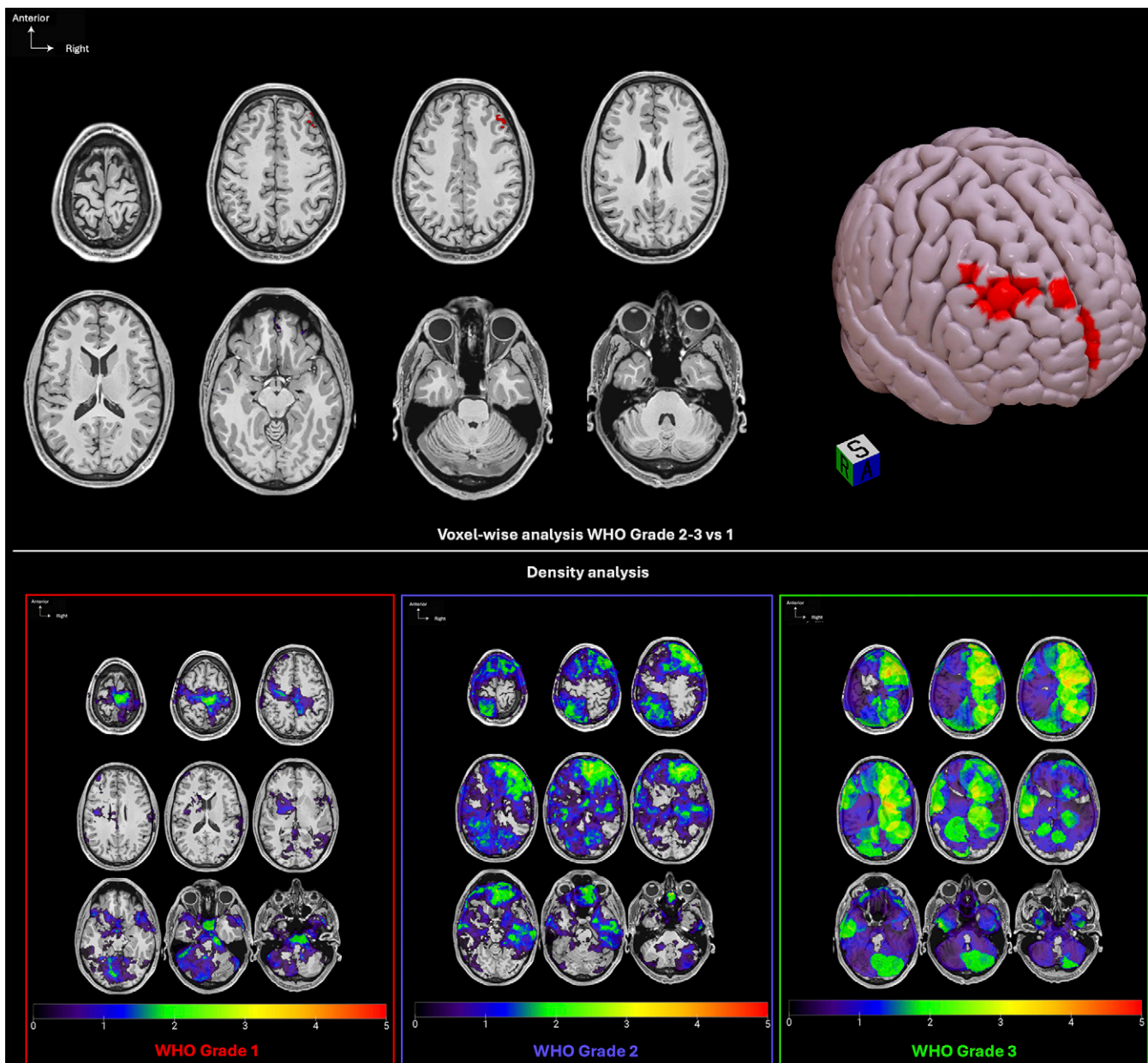


Figure 8: Density and voxelwise analysis of meningioma on the basis of tumor grade. Density maps and voxelwise analyses are shown for resected meningiomas with available histology, comparing World Health Organization (WHO) grade 2–3 tumors versus WHO grade 1 tumors. Colored voxels (red) indicate regions surviving whole-brain multiple-comparison correction ($q < .05$). Images are displayed in Montreal Neurological Institute 152 space using neurologic convention.

- Bi WL, Santagata S. Skull Base Tumors: Neuropathology and Clinical Implications. *Neurosurgery* 2022;90(3):243–261.
- Whittle IR, Smith C, Navoo P, Collie D. Meningiomas. *Lancet* 2004;363(9420):1535–1543.
- Guo C, Xue Y, Li Y, Tian Q, Qu Y, Cai Q. Risk factors for motor decline following parasagittal and falx meningioma resection in the middle third. *Front Oncol* 2025;15:1458934.
- Patel RV, Yao S, Aguilar Murillo E, Huang RY, Bi WL. Spatial Distribution of Meningiomas: A Magnetic Resonance Image Atlas. *Neurosurgery* 2025;96(4):769–778.
- Hirayama R, Kinoshita M, Arita H, et al. Voxel-based lesion mapping of meningioma: a comprehensive lesion location mapping of 260 lesions. *J Neurosurg* 2018;128(6):1707–1712.
- Sun C, Dou Z, Wu J, et al. The Preferred Locations of Meningioma According to Different Biological Characteristics Based on Voxel-Wise Analysis. *Front Oncol* 2020;10:1412.
- Evans AC, Janke AL, Collins DL, Baillet S. Brain templates and atlases. *Neuroimage* 2012;62(2):911–922.
- Roux A, Roca P, Edjlali M, et al. MRI Atlas of IDH Wild-Type Supratentorial Glioblastoma: Probabilistic Maps of Phenotype, Management, and Outcomes. *Radiology* 2019;293(3):633–643.
- De Witt Hamer PC, Hendriks EJ, Mandonnet E, Barkhof F, Zwinderman AH, Duffau H. Resection probability maps for quality assessment of glioma surgery without brain location bias. *PLoS One* 2013;8(9):e73353.
- Louis DN, Perry A, Wesseling P, et al. The 2021 WHO classification of tumors of the central nervous system: A summary. *Neuro Oncol* 2021;23(8):1231–1251.
- Simpson D. The recurrence of intracranial meningiomas after surgical treatment. *J Neurol Neurosurg Psychiatry* 1957;20(1):22–39.
- Ripollés P, Marco-Pallarés J, de Diego-Balaguer R, et al. Analysis of automated methods for spatial normalization of lesioned brains. *Neuroimage* 2012;60(2):1296–1306.
- Brett M, Leff AP, Rorden C, Ashburner J. Spatial normalization of brain images with focal lesions using cost function masking. *Neuroimage* 2001;14(2):486–500.
- Pariset S, Darlix A, Baumann C, et al. A Probabilistic Atlas of Diffuse WHO Grade II Glioma Locations in the Brain. *PLoS One* 2016;11(1):e0144200.

20. Lee JW, Wen PY, Hurwitz S, et al. Morphological characteristics of brain tumors causing seizures. *Arch Neurol* 2010;67(3):336–342.
21. Li H, Nickerson LD, Xiong J, et al. A high performance 3D cluster-based test of unsmoothed fMRI data. *Neuroimage* 2014;98:537–546.
22. Li H, Nickerson LD, Zhao X, Nichols TE, Gao JH. A voxelation-corrected non-stationary 3D cluster-size test based on random field theory. *Neuroimage* 2015;118:676–682.
23. Hosainey SAM, Bouget D, Reinertsen I, et al. Are there predilection sites for intracranial meningioma? A population-based atlas. *Neurosurg Rev* 2022;45(2):1543–1552.
24. Bommakanti K, Somayajula S, Suvarna A, et al. Pre-operative and post-operative cognitive deficits in patients with supratentorial meningiomas. *Clin Neurol Neurosurg* 2016;143:150–158.
25. Frenkel-Toledo S, Levin MF, Berman S, et al. Shared and distinct voxel-based lesion-symptom mappings for spasticity and impaired movement in the hemiparetic upper limb. *Sci Rep* 2022;12(1):10169.
26. Elbadry Ahmed R, Tang H, Asemota A, Huang L, Boling W, Bannout F. Meningioma Related Epilepsy- Pathophysiology, Pre/postoperative Seizures Predicators and Treatment. *Front Oncol* 2022;12:905976.
27. Khan MF, Patel S, Alnasser AA, et al. Predicting epilepsy in patients diagnosed with intracranial meningiomas: A systematic review and meta-analysis of clinical and anatomical risk factors. *J Clin Neurosci* 2025;139:111451.
28. Teske N, Teske NC, Greve T, et al. Perifocal edema is a risk factor for preoperative seizures in patients with meningioma WHO grade 2 and 3. *Acta Neurochir (Wien)* 2024;166(1):170.
29. Englot DJ, Magill ST, Han SJ, Chang EF, Berger MS, McDermott MW. Seizures in supratentorial meningioma: a systematic review and meta-analysis. *J Neurosurg* 2016;124(6):1552–1561.
30. Chen WC, Magill ST, Englot DJ, et al. Factors Associated With Pre- and Postoperative Seizures in 1033 Patients Undergoing Supratentorial Meningioma Resection. *Neurosurgery* 2017;81(2):297–306.
31. Akhavan-Sigari R, Mazloum Farsi BafM, Ariabod V, Rohde V, Rahighi S. Connection between Cell Phone use, p53 Gene Expression in Different Zones of Glioblastoma Multiforme and Survival Prognoses. *Rare Tumors* 2014;6(3):5350.